

Quantum turbulence visualized by particle dynamics

M. La Mantia* and L. Skrbek

Faculty of Mathematics and Physics, Charles University, Ke Karlovu 3, 121 16 Prague, Czech Republic

(Received 29 May 2014; revised manuscript received 10 July 2014; published 29 July 2014)

The Lagrangian dynamics of micrometer-sized solid particles of hydrogen and deuterium is investigated in thermal counterflow of superfluid ^4He at length scales ℓ_{exp} straddling about two orders of magnitude across the average distance ℓ between quantized vortices by using the particle tracking velocimetry technique. The normalized probability distribution functions of the particle velocities and accelerations change from the shapes typical of quantum turbulence, characterized by power-law tails, at length scales $\ell_{\text{exp}} \lesssim \ell$, to forms similar to those obtained in classical turbulent flows, at $\ell_{\text{exp}} \gtrsim \ell$, although the power-law behavior of the acceleration distribution tails is less clear than that observed for the particle velocities. Moreover, the acceleration distribution follows a nearly log-normal, classical-like shape, at $\ell \lesssim \ell_{\text{exp}} \lesssim L_{\text{int}}$, where L_{int} denotes the integral length scale, providing thus, within the just defined inertial range, experimental evidence of the existence of classical-like, macroscopic vortical structures in thermal counterflow of superfluid ^4He , which is traditionally regarded as a quantum flow with no obvious classical analog. Additionally, we report our observations of the added mass effect in quantum turbulence and discuss them in the framework of a developed model of particle dynamics.

DOI: [10.1103/PhysRevB.90.014519](https://doi.org/10.1103/PhysRevB.90.014519)

PACS number(s): 67.25.dk, 47.37.+q, 47.27.-i

I. INTRODUCTION

Quantum turbulence can loosely be defined as the most general form of motion of quantum fluids displaying superfluidity. Their physical properties cannot be described by classical physics but depend on quantum mechanics [1,2]. At finite temperature, quantum fluids, such as superfluid ^4He , also known as He II, display the two-fluid behavior and, on the phenomenological level, are viewed as consisting of two interpenetrating fluids. The gas of thermal excitations—the viscous normal component—carries the entire entropy content of the quantum fluid, while the superfluid component is assumed inviscid and its circulation quantized in units of the quantum of circulation $\kappa = h/m_{\text{sp}}$, where h is the Planck constant and m_{sp} denotes the mass of the superfluid particle, e.g., the mass of the ^4He atom. Quantized vortices can then exist in superfluids (singly quantized in the case of He II) and are usually arranged in a tangle, whose dynamical behavior is an essential ingredient of quantum turbulence.

Recent progress in quantum turbulence—a fast developing branch of fluid dynamics—has been especially stimulated by the implementation of contemporary flow visualization techniques [3] to the study of quantum flows of He II [4–7], as these techniques allow tracing the motion of small particles suspended in a fluid (the particles reflect the light of a laser beam and their time-dependent positions are captured, for example, by a fast digital camera). Fundamental results have been obtained by visualizing the dynamics of hydrogen and deuterium particles of micrometer size. Their motion is very complex, as in quantum turbulence, particles interact with both the normal and superfluid velocity fields simultaneously and may become trapped (and/or detrapped) onto the cores of quantized vortices. Both the normal and superfluid velocity fields can become turbulent and are coupled by the action of the mutual friction force [1,2,7].

The application of the particle tracking velocimetry (PTV) technique resulted specifically in the discovery of nonclassical velocity statistics in decaying [8] and stationary thermal counterflow [9,10] of He II, among other results, such as direct observations of quantized vortex reconnections [11] and Kelvin waves [12]. Recently, we have confirmed experimentally the computational prediction of a crossover between classical and quantum features in the velocity distribution of steady-state thermal counterflow, which was probed at various length scales ℓ_{exp} , smaller and larger than the average distance ℓ between quantized vortices [13]. Note that the latter scale can be viewed as proportional to the quantum length scale $\ell_Q \approx 2\pi(\varepsilon/\kappa^3)^{-1/4}$, where ε is the energy decay rate [1,14].

A step forward has been to focus on particle accelerations in quantum flows [10], as this research field is well established in classical fluid mechanics [15]. This paper extends our recent work on deuterium particle accelerations [10] in vertical thermal counterflow, where, at $\ell_{\text{exp}} \approx \ell$, we found that the normalized probability density function (PDF) of the instantaneous acceleration a_z in the vertical direction can be approximated by the classical-like form

$$\text{PDF} = \frac{\exp(3s^2/2)}{4\sqrt{3}} \left[1 - \text{erf} \left(\frac{\ln|a/\sqrt{3}| + 2s^2}{\sqrt{2}s} \right) \right], \quad (1)$$

where $s = 1$ and $a = (a_z - \bar{a}_z)/a_z^{\text{sd}}$, with \bar{a}_z and a_z^{sd} being the mean and standard deviation of the dimensional acceleration a_z , respectively. This functional form, associated with a log-normal distribution of the acceleration magnitude, has been reported by Mordant *et al.* [16] in their study on the dynamics of fluid particles in classical turbulence, while the results of Qureshi *et al.* [17,18] refer to inertial particles and are consistent with $s = 0.62$. Note, however, that such a log-normal behavior does not have a clear physical interpretation and may be linked to the fact that classical vortices, unlike quantized ones, have arbitrary strength (see, e.g., [19] for an alternative, multifractal description of the problem).

This paper shows that the experimental results on particle accelerations, similarly to those on velocities [13], depend on

*lamantia@nbox.troja.mff.cuni.cz

the length scale ℓ_{exp} at which the stationary thermal counterflow is probed and, consequently, display either quantum, at $\ell_{\text{exp}} \lesssim \ell$, or classical, at $\ell_{\text{exp}} \gtrsim \ell$, features. The size of the particle, $d \approx \ell/10$, represents the smallest physical length scale we can access, providing that the images are taken fast enough, so that the particle between two successively taken frames does not move further than its size. The upper length-scale limit is determined by the lengths of the particle trajectories that we can follow. In order to directly compare visualization studies on velocity and acceleration, the quantum flow under study is the same [13], i.e., steady-state thermal counterflow [1,2] of He II, generated by a flat square heater placed on the bottom of our vertical channel. This allows selecting a suitable quantum length scale, by tuning the heat flux q per unit area. The superfluid component of He II moves towards the heater where it converts into the normal component that flows away from it. Above a (small) critical velocity v_c , the counterflow velocity $v_{\text{ns}} = q/(\rho_s \sigma T)$ generates a tangle of quantized vortex lines with density $L = [\gamma(T)(v_{\text{ns}} - v_c)]^2 \approx \ell^{-2}$, where $\gamma(T)$ is known with sufficient accuracy (ρ_s is the superfluid density, σ indicates the entropy per unit volume, and T denotes the temperature).

II. EXPERIMENTAL SETUP AND PROTOCOL

We use the Prague experimental visualization setup already described in our previous publications [9,10,13]. It consists of a custom-built optical cryostat, a purpose-made seeding system supplying micrometer-sized solid particles (generated by mixing helium and deuterium, or hydrogen, gases at room temperature and injecting the mixture into the helium bath), a continuous-wave laser and cylindrical optics, in order to obtain a thin laser sheet of about 10 mm high and less than 1 mm thick, and a fast digital camera situated perpendicularly to the laser sheet, focused on a 12.8 by 8 mm field of view. The PTV technique is used for the measurement of Lagrangian quantities in a vertical plane, in the middle of the square experimental channel of 25 mm sides and about 100 mm long. The gaseous mixture is injected into the helium bath that is then brought to some chosen temperature. As both hydrogen and deuterium particles are not neutrally buoyant, images are recorded in order to estimate their settling velocities and dimensions, which are of a few micrometers [9,13]. The heater is then switched on, images collected (each movie is typically made of a few thousand images), and the particle tracks are computed by using an open-source algorithm [20].

The trajectories obtained from the images are filtered by using a dedicated computer program in order to remove spurious tracks before calculating velocities and accelerations. The latter are computed by interpolating linearly consecutive position differences, in the case of velocities, and velocity differences, in the case of accelerations, by purpose-made computer programs (the obtained accelerations are therefore linearly related to the particle velocity differences). Note also that the distance between particles along the trajectories, which can be seen as a measure of the probed length scale, is proportional to the time between successive frames, i.e., it decreases as the frame rate increases. Besides, particle positions at a low frame rate can also be obtained by accordingly removing particle positions from data sets recorded

at a high frame rate, not only from images recorded at a low frame rate. This procedure is, in fact, better, as the particle tracks are confidently known, being already identified using dense particle positions from high frame rate movies. The Lagrangian quantities calculated from several movies obtained under the same experimental conditions are finally combined. Although our data processing approach is simpler than some employed for the Lagrangian analysis of classical turbulent flows [21–23], the calculated velocities and accelerations appear consistent with the proposed physical description of the problem.

The probed length scale ℓ_{exp} is quantified by introducing the nondimensional time $\tau = t_1/t_2$, where t_1 is the time interval used for the calculation of the particle velocities and accelerations along the tracks, which, as explained above, is equal to, or larger than, the time between two successive images taken by the camera, and $t_2 = \ell/V_{\text{abs}}$, where V_{abs} denotes the mean particle velocity obtained under the considered experimental conditions, at the smallest t_1 , i.e., t_2 represents the time that a particle moving with the mean velocity V_{abs} takes to travel the distance ℓ , in other words, $\ell_{\text{exp}} \approx \ell$, if $t_1 \approx t_2$. For a more detailed discussion on the experimental setup and procedure, we direct the reader to our previous works [9,10,13].

III. ACCELERATION STATISTICS

We have argued in [13] that, for $\ell_{\text{exp}} \ll \ell$, the power-law shape of the velocity PDF tails in quantum turbulence follows from the simple assumption that, close to a singly quantized vortex, the superfluid velocity $v_s = \kappa/(2\pi r)$, where r is the distance from the vortex core. If the probability $P_v(v)$ of observing a velocity v is assumed proportional to $\int \delta(v - v_s) r dr$, where δ denotes the delta function, it follows that $P_v(v) \propto v^{-3}$ [24–26]. Here, we are extending this reasoning by assuming that the probability $P_a(a)$ of observing an acceleration a is proportional to $\int \delta(a - a_s) r dr$ and, as in the proximity of a quantized vortex, the superfluid acceleration $a_s = v_s^2/r$ (see, e.g., [27]), it follows that $P_a(a) \propto a^{-5/3}$ [24,26]. We stress that the influence of the normal-fluid velocity field and superfluid velocity field due to other quantized vortices is neglected here, i.e., the necessary condition is $\ell_{\text{exp}} \ll \ell$.

As we stated in [13], within the investigated range of parameters, the character of the observed particle tracks, moving upwards and/or downwards in steady-state thermal counterflow, appears very similar. It is not possible to easily identify particles trapped into quantized vortex lines. We therefore report the statistical investigation of the particle dynamics.

Our typical experimental results are shown in Fig. 1, where the normalized acceleration distribution $(a_x - \bar{a}_x)/a_x^{\text{sd}}$, computed at various ℓ_{exp} , for both hydrogen and deuterium particles, is plotted (\bar{a}_x and a_x^{sd} are the mean and standard deviation, respectively, of the instantaneous dimensional acceleration a_x in the horizontal direction, perpendicular to the mean counterflow velocity v_{ns}). First of all (see especially the inset of Fig. 1), we report the result that the distribution of the particle acceleration a , at length scales about one order of magnitude smaller than ℓ , is indeed found to be consistent with the law that predicts tails of $a^{-5/3}$ form, on the basis of

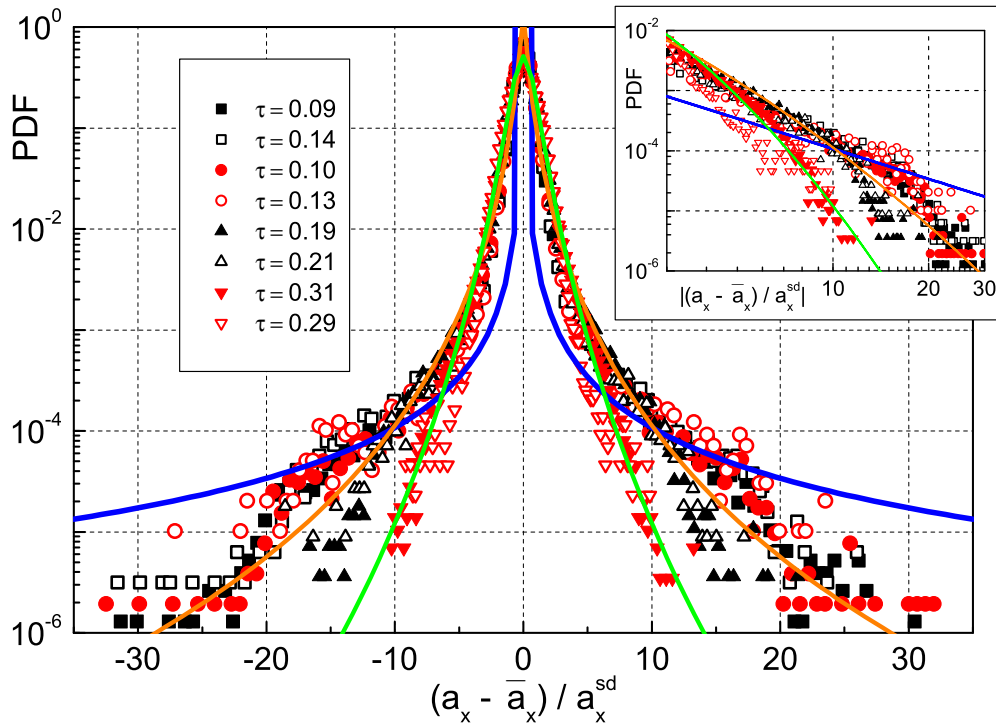


FIG. 1. (Color online) PDF of $(a_x - \bar{a}_x)/a_x^{sd}$. Tracks with at least five points. Number of trajectory points: at least 1.9×10^5 , up to 12.3×10^5 ; see also Table I. The area below the data curves is normalized to 1. Filled symbols refer to hydrogen particles, while open symbols denote deuterium particles. Black \blacksquare : images taken at 400 fps, $T = 1.77$ K, $q = 612$ W/m 2 , $\ell = 70$ μ m, $V_{\text{abs}} = 2.46$ mm/s; black \square : 400 fps, $T = 1.77$ K, $q = 608$ W/m 2 , $\ell = 70$ μ m, $V_{\text{abs}} = 3.91$ mm/s; red \bullet : 400 fps, $T = 1.66$ K, $q = 490$ W/m 2 , $\ell = 75$ μ m, $V_{\text{abs}} = 3.02$ mm/s; red \circ : 400 fps, $T = 1.65$ K, $q = 487$ W/m 2 , $\ell = 74$ μ m, $V_{\text{abs}} = 3.76$ mm/s; black \blacktriangle : 200 fps, $T = 1.66$ K, $q = 489$ W/m 2 , $\ell = 75$ μ m, $V_{\text{abs}} = 2.90$ mm/s; black \triangle : 200 fps, $T = 1.65$ K, $q = 490$ W/m 2 , $\ell = 73$ μ m, $V_{\text{abs}} = 3.15$ mm/s; red \blacktriangledown : 100 fps, $T = 1.66$ K, $q = 489$ W/m 2 , $\ell = 75$ μ m, $V_{\text{abs}} = 2.34$ mm/s; red ∇ : 100 fps, $T = 1.66$ K, $q = 492$ W/m 2 , $\ell = 74$ μ m, $V_{\text{abs}} = 2.13$ mm/s; blue line: power-law fit, $0.005|(a_x - \bar{a}_x)/a_x^{sd}|^{-5/3}$; orange line: log-normal fit, given by Eq. (1), with $s = 1$ and $a = (a_x - \bar{a}_x)/a_x^{sd}$; green line: log-normal fit, given by Eq. (1), with $s = 0.62$ and $a = (a_x - \bar{a}_x)/a_x^{sd}$. Inset: Log-log plot of the PDF of $|(a_x - \bar{a}_x)/a_x^{sd}|$; symbols as in the main panel.

the quantum description of superfluid ^4He , although the latter power-law behavior is less clear than that observed in the case of velocities [13].

Figure 2 displays the evolution of the acceleration PDF obtained at different τ under the same experimental conditions. We see that, as t_1 increases, the PDF changes its shape to a nearly classical-like one, i.e., the crossover reported in [13] for the velocity distribution is here confirmed in the case of the particle accelerations. Besides, the outcome may be seen as indicating the occurrence of classical-like turbulent behavior in quantum turbulence, at length scales larger than ℓ , i.e., as an indirect evidence of the existence of macroscopic vortical structures in thermal counterflow of He II, which is a quantum flow without any obvious classical analog. This is especially relevant as in the bulk of thermally driven quantum flows the coherent motion of bundles of quantized vortices has been until now investigated only in numerical simulations; see, e.g., [28] and references therein.

Consider that the velocity difference PDF, at scales exceeding, or of the order of, the integral scale L_{int} , is found to be of a nearly Gaussian shape in classical turbulent flows [24,29,30]. Such a scale can be obtained from the velocity autocorrelation function. In the present analysis, however, it could not be calculated precisely, mainly due to the limited size of the data sets at large τ . Nevertheless, the integral length scale appears to be of the same order of, or larger than, ℓ_{exp} , at

the largest achievable τ , which is much smaller (about two orders of magnitude) than that corresponding to a particle traveling across the entire channel width. Note also that in Fig. 2 the core of the corresponding distribution, which contains the vast majority of the data set points, has a Gaussian form, while, at smaller scales, the distribution core is clearly non-Gaussian. Additionally, as shown in Fig. 3, the normalized distribution of the particle velocity u in the horizontal direction, obtained for the same data set, is already nearly Gaussian at $\tau \approx 2$, confirming thus that our recent results on the velocity distribution crossover [13], found with solid deuterium particles, hold also in the case of hydrogen particles.

The previous discussion consequently supports the claim that at length scales larger than ℓ and smaller than L_{int} , i.e., in a quasi-inertial range of scales, we are observing a classical-like turbulent behavior of a quantum flow, as, at $\tau \approx 10$, the particle velocity and acceleration distributions both have classical-like forms.

The recent numerical results by Baggaley and Barenghi [26] on acceleration statistics also support our experimental findings. At the investigated length scales, equal to about 0.3ℓ , their distributions appear to have Gaussian (log-normal) cores for velocity (acceleration) and power-law tails, that is, the computational outcome qualitatively agrees with the experimental data.

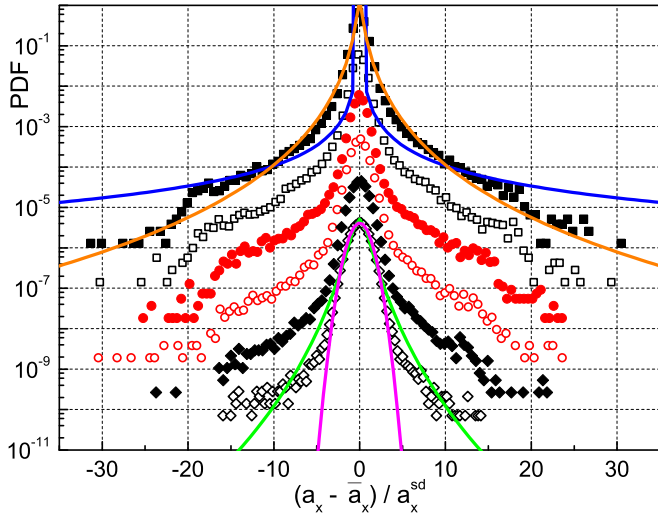


FIG. 2. (Color online) Evolution of the PDF of $(a_x - \bar{a}_x)/a_x^{\text{sd}}$ with τ . Hydrogen particles data collected at 400 fps, $T = 1.77$ K, $q = 612$ W/m², $\ell = 70$ μm , $V_{\text{abs}} = 2.46$ mm/s. Black \blacksquare : $t_1 = 2.5$ ms, $\tau = 0.09$ (each subsequent data set shifted down by one decade); black \square : $t_1 = 5$ ms, $\tau = 0.18$; red \bullet : $t_1 = 10$ ms, $\tau = 0.35$; red \circ : $t_1 = 25$ ms, $\tau = 0.88$; black \blacklozenge : $t_1 = 50$ ms, $\tau = 1.77$; black \diamond : $t_1 = 250$ ms, $\tau = 8.83$; blue line: power-law fit, $0.005|(a_x - \bar{a}_x)/a_x^{\text{sd}}|^{-5/3}$; orange line: log-normal fit, given by Eq. (1), with $s = 1$ and $a = (a_x - \bar{a}_x)/a_x^{\text{sd}}$; green line: log-normal fit, given by Eq. (1), with $s = 0.62$ and $a = (a_x - \bar{a}_x)/a_x^{\text{sd}}$ (shifted down by five decades); magenta line: Gaussian fit of the black \diamond data set (shifted down by five decades).

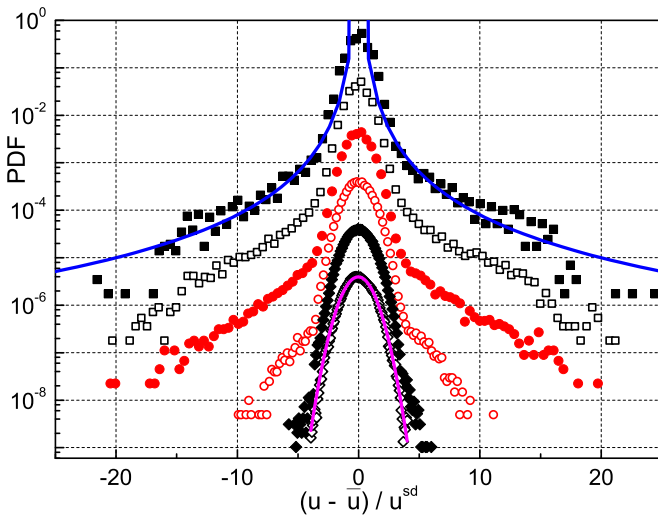


FIG. 3. (Color online) Evolution of the PDF of $(u - \bar{u})/u^{\text{sd}}$ with τ , where \bar{u} and u^{sd} are the mean and standard deviation of the dimensional particle velocity u in the horizontal direction, respectively. Hydrogen particles data collected at 400 fps, $T = 1.77$ K, $q = 612$ W/m², $\ell = 70$ μm , $V_{\text{abs}} = 2.46$ mm/s. Black \blacksquare : $t_1 = 2.5$ ms, $\tau = 0.09$ (each subsequent data set shifted down by one decade); black \square : $t_1 = 5$ ms, $\tau = 0.18$; red \bullet : $t_1 = 10$ ms, $\tau = 0.35$; red \circ : $t_1 = 25$ ms, $\tau = 0.88$; black \blacklozenge : $t_1 = 50$ ms, $\tau = 1.77$; black \diamond : $t_1 = 250$ ms, $\tau = 8.83$; blue line: power-law fit, $0.008|(u - \bar{u})/u^{\text{sd}}|^{-3}$; magenta line: Gaussian fit of the black \diamond data set (shifted down by five decades).

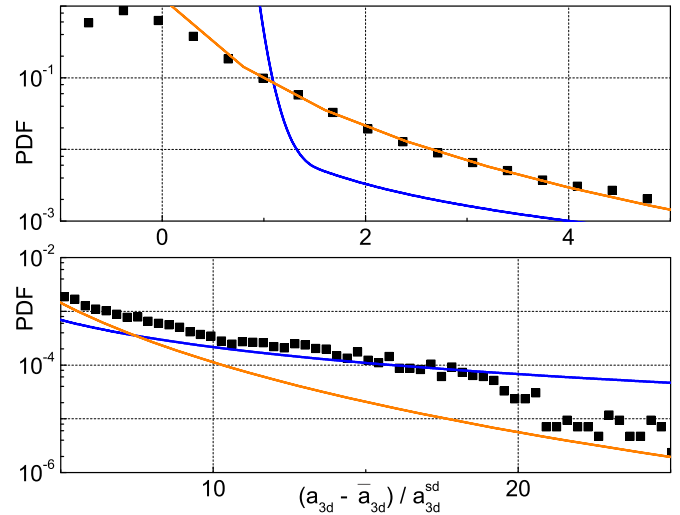


FIG. 4. (Color online) PDF of $(a_{3d} - \bar{a}_{3d})/a_{3d}^{\text{sd}}$, where \bar{a}_{3d} and a_{3d}^{sd} are the mean and standard deviation of the three-dimensional acceleration magnitude $a_{3d} = \sqrt{2a_x^2 + a_z^2}$, respectively. Hydrogen particles data collected at 400 fps, $T = 1.77$ K, $q = 612$ W/m², $\ell = 70$ μm , $V_{\text{abs}} = 2.46$ mm/s. Black \blacksquare : $t_1 = 2.5$ ms, $\tau = 0.09$; blue line: power-law fit, $0.01[(a_{3d} - \bar{a}_{3d})/a_{3d}^{\text{sd}}]^{-5/3}$; orange line: log-normal fit, given by Eq. (1), with $s = 1$ and $a = (a_{3d} - \bar{a}_{3d})/a_{3d}^{\text{sd}}$.

At length scales smaller than ℓ , the departure from the log-normal shape is observed at the largest accelerations, when the particles are, on average, closer to the quantized vortices. As shown in Figs. 1 and 2, this is consistent with the prediction for the tails up to about $20|a_x^{\text{sd}}|$, which approximately corresponds to the acceleration of a few micrometer-sized particle touching a vortex core (note that the particle size d has a large influence on the acceleration magnitude as $a \propto d^{-3}$). This could also explain why the acceleration power-law behavior is less clear than that observed in the case of velocities. In other words, smaller particles should lead to acceleration distributions with more pronounced power-law tails, assuming the flow is being probed at small enough scales.

As recently discussed by us [13], the statistical distributions of the particle velocity in the vertical direction are affected by the imposed vertical counterflow velocities of He II and show less noticeable departures from the classical shapes at scales smaller than ℓ . The same behavior is observed for the acceleration distributions, as recently shown in [7] in the case of deuterium particles (hydrogen particles behave similarly). However, the power-law tails can also be seen if the normalized distribution of the particle three-dimensional acceleration magnitude $a_{3d} = \sqrt{2a_x^2 + a_z^2}$ is plotted, as displayed in Fig. 4 for a sample case, at $\ell_{\text{exp}} < \ell$.

IV. ADDED MASS EFFECT

Having identified the quantum and classical signatures in both velocity and acceleration distributions, the following step was to analyze the role of inertia in the dynamics of hydrogen/deuterium particles in thermal counterflow, taking into account the two-fluid behavior of quantum fluids. A deeper quest must consider the added mass problem; see, e.g., [31] and references therein. In order to appreciate its physical meaning,

we start by considering it in its simplest case, in an inviscid fluid.

The equation of motion of a particle p , of unit volume, in a fluid f , can be written as

$$\rho_p \frac{du_p}{dt} = \rho_f \frac{Du_f}{Dt} + C\rho_f \left(\frac{Du_f}{Dt} - \frac{du_p}{dt} \right), \quad (2)$$

where u is the instantaneous velocity vector and ρ indicates the density. The dimensionless quantity C is known as the added mass coefficient, equal to $1/2$ for a spherical particle. The particle acceleration is assumed to be only a function of time t , i.e., the particle dimensions are assumed much smaller than the relevant length scales of the considered flow, while the fluid acceleration depends on both time and space. Stokes drag, buoyancy force, and other forces (see, e.g., [6,32]) are neglected here.

Let us write Eq. (2) in a slightly different form, i.e.,

$$\frac{du_p}{dt} = \frac{1+C}{\rho_p/\rho_f + C} \frac{Du_f}{Dt} = K_p \frac{Du_f}{Dt}, \quad (3)$$

where K_p can be seen as the ratio between particle and fluid accelerations. From this equation, the following conclusions can be drawn: (i) if $\rho_p = \rho_f$, $K_p = 1$, i.e., the particle has the same acceleration as the fluid; (ii) if $\rho_p > \rho_f$, $K_p < 1$, i.e., the particle accelerates less than the fluid; (iii) if $\rho_p < \rho_f$, $K_p > 1$, i.e., the particle accelerates more than the fluid, until the limiting case, $\rho_p \ll \rho_f$, when, e.g., a spherical particle ($C = 1/2$) accelerates three times faster than the fluid (a negative ion, a spherical empty bubble in He II [33], closely corresponds to this limit).

It is useful to consider the consequences of this simple analysis for flow visualization experiments at very low temperatures (He II density $\rho_f \approx 145 \text{ kg/m}^3$), where there is no normal-fluid component, assuming the use of spherical particles of solid hydrogen, of density $\rho_H \approx 88 \text{ kg/m}^3$, and deuterium, of density $\rho_D \approx 200 \text{ kg/m}^3$. It follows that $K_H \approx 1.36$ and $K_D \approx 0.80$, i.e., in the same quantum flow, spherical hydrogen particles ought to accelerate about $K_H/K_D \approx 1.70$ times faster than deuterium particles.

In order to appreciate the effect of the shape of the particles on their acceleration, let us consider a prolate spheroid of major axis M and minor axis m , in which case C can be calculated analytically; see, e.g., [34]. If the particle is accelerating in the direction of the major axis and $M = 2m$ ($M = 5m$), we find that hydrogen particles in He II accelerate about 1.94 (2.16) times more than deuterium particles. If the same prolate spheroid is instead accelerating in the direction of the minor axis, the same hydrogen particles accelerate about 1.59 (1.51) times more than deuterium particles. We see that, under the assumptions of the present model, hydrogen particles in He II at very low temperature are expected to accelerate roughly 1.5 to 2 times more rapidly than deuterium particles.

Let us now consider the case of a spherical particle of unit volume in a classical viscous flow. The corresponding equation of motion can be obtained by taking into account the buoyancy force and Stokes drag and neglecting other forces; see, e.g., [32] for a detailed discussion on its derivation.

Equation (3) is then rewritten as

$$\frac{du_p}{dt} = K_p \frac{Du_f}{Dt} + Bg + S(u_f - u_p), \quad (4)$$

where g is the acceleration due to gravity and $K_p = 1.5/(\rho_p/\rho_f + 0.5) = 1.5\rho_f/\rho_0$. The second term on the right-hand side of Eq. (4) denotes the buoyancy force, with $B = (\rho_p/\rho_f - 1)/(\rho_p/\rho_f + 0.5) = (\rho_p - \rho_f)/\rho_0$, while the third term represents the Stokes drag, with $S = 6\pi\mu R_p/[V_p(\rho_p + 0.5\rho_f)] = 9\mu/(2R_p^2\rho_0)$, where μ is the fluid dynamic viscosity, R_p indicates the particle radius, and V_p denotes its volume.

The fluid acceleration per unit volume can generally be written as

$$\rho_f \frac{Du_f}{Dt} = -\nabla P + \mu \nabla^2 u_f + F, \quad (5)$$

where P is the fluid pressure and F indicates other body forces. Note that, for an inviscid fluid, the second term on the right-hand side of Eq. (5) vanishes and in the vicinity of a vortex, also neglecting F , Eq. (5) becomes $\rho_f Du_f/Dt = -\nabla P$.

In the case of a spherical particle moving in superfluid ^4He , the two-fluid description of He II can be used to reformulate Eq. (4) as

$$\frac{du_p}{dt} = K_p \left(\frac{\rho_n}{\rho_f} \frac{Du_n}{Dt} + \frac{\rho_s}{\rho_f} \frac{Du_s}{Dt} \right) + Bg + S(u_n - u_p), \quad (6)$$

where the subscripts n and s indicate the normal and superfluid components of He II, respectively, S becomes $9\mu_n/(2R_p^2\rho_0)$, and the total fluid density ρ_f is equal to the sum of ρ_n and ρ_s . If it is also assumed that

$$\frac{Du_f}{Dt} = \left(\frac{\rho_n}{\rho_f} \frac{Du_n}{Dt} + \frac{\rho_s}{\rho_f} \frac{Du_s}{Dt} \right), \quad (7)$$

then Eq. (6) is analogous to Eq. (4) and can be rewritten more conveniently as

$$\frac{du_p}{dt} - Bg - S(u_n - u_p) = K_p \frac{Du_f}{Dt}, \quad (8)$$

in order to allow comparisons with experimental data.

The ratio between the accelerations of hydrogen and deuterium particles in the same experimental conditions can then be evaluated from suitable ensemble averages of the left-hand side of Eq. (8) and, finally, compared to $K_H/K_D \approx 1.70$. This is done by using instantaneous values of particle velocity and acceleration and postulating adequate values of particle radius and fluid velocity. In the case of vertical thermal counterflow, the latter normal-fluid velocity is assumed null in the horizontal direction and equal to its mean value in the vertical direction, while the mean particle radius can be either assumed or obtained experimentally from the particle settling velocities, following the procedure described in [9,13].

More specifically, the ratio RA between the amplitudes of the three-dimensional acceleration of hydrogen, H , and deuterium, D , particles can be written as

$$RA = \frac{(\sqrt{2A_h^2 + A_v^2})_H}{(\sqrt{2A_h^2 + A_v^2})_D}, \quad (9)$$

TABLE I. Ratio RA between the amplitudes of the three-dimensional acceleration of hydrogen, H, and deuterium, D, particles, computed as detailed in the text, to be compared to $K_H/K_D \approx 1.70$. Heat flux q_p (W/m^2), temperature T_p (K), camera frame rate f (fps), number N_p of track points (10^5). If the particle radius R_p (μm) was obtained experimentally, following the procedure described in [9,13], its mean value was used in the computations (its standard deviation is also shown in the table, as for RA).

q_H	q_D	T_H	T_D	f	N_H	N_D	R_H	R_D	RA
612	608	1.77	1.77	400	12.3	5.5	2.7 ± 0.8	2.6 ± 1.0	2.28 ± 1.49
490	487	1.66	1.65	400	8.0	1.9	2.7 ± 0.8	5.2 ± 1.3	7.95 ± 5.81
490	487	1.66	1.65	400	8.0	1.9	2.5	2.5	1.81 ± 1.56
489	490	1.66	1.65	200	7.2	3.1	2.7 ± 0.8	5.2 ± 1.3	9.94 ± 8.21
489	490	1.66	1.65	200	7.2	3.1	2.5	2.5	2.09 ± 2.05
489	492	1.66	1.66	100	12.2	2.3	2.7 ± 0.8	5.2 ± 1.3	11.57 ± 9.34
489	492	1.66	1.66	100	12.2	2.3	2.5	2.5	2.17 ± 2.21
481	490	1.68	1.65	200	3.4	3.1	2.5	2.5	3.03 ± 2.28
481	492	1.68	1.66	100	2.0	2.3	2.5	2.5	1.98 ± 2.07

where the subscripts h and v indicate the horizontal and vertical thermal counterflow directions, respectively, and A denotes relevant ensemble averages of the left-hand side of Eq. (8).

The outcome is shown in Table I. It is clear that the proposed model qualitatively agrees with the experimental data, as the acceleration of hydrogen particles is always found to be larger than that of deuterium particles, i.e., $RA \gtrsim 1.5$. The quantitative agreement is less satisfactory and this may be due to various reasons. For example, the particles are, in general, not spherical and occasionally rotate [9]. Besides, other forces may affect their motion; see, e.g., [32] for a detailed discussion on the issue. Note also that deuterium particles prepared under the same experimental conditions tend to be larger than hydrogen particles [9] and that the particle radius significantly influences the value of RA (for example, the drag experienced by the largest particles is likely not accurately estimated by the Stokes drag approximation).

V. CONCLUSIONS

Our study on the dynamics of hydrogen and deuterium particles visualizing quantum turbulence in counterflowing superfluid ^4He provides direct experimental evidence that both quantum and classical characteristics of turbulence can be detected simultaneously when quantum turbulence is probed at small and large length scales, where coarse graining over a number of quantized building blocks—singly quantized vortices—implies classical behavior. Our acceleration studies

also reveal the importance of the added mass effect in quantum turbulence, in qualitative agreement with the developed model of particle dynamics. Quantum and inertial effects, together with the finite size of the particles, shape not only the distribution of the velocity v , characterized by v^{-3} tails and a classical Gaussian core [13], but also, as shown here experimentally, the distribution of the acceleration a , having tails of $a^{-5/3}$ form, of predictable width, and a classical log-normal core, although the power-law behavior of the acceleration distribution tails is less clear than that obtained for the velocities. Remarkably, at scales larger than the mean distance between quantized vortices but not exceeding the integral length scale of the flow, i.e., within a quasi-inertial range of scales, the shape of the acceleration PDF strongly suggests the existence of macroscopic vortical structures in thermal counterflow of He II. In other words, taking into account the statistical distributions of both particle velocities and accelerations, we observe a classical turbulent behavior of a steady quantum flow that does not have any direct classical analog. This confirms the robustness of the principles and phenomenology of hydrodynamic turbulence.

ACKNOWLEDGMENTS

We thank L. Biferale, M. Bourgoïn, D. Duda, M. P. Rast, M. Rotter, K. R. Sreenivasan and J. Věražka for fruitful discussions and valuable help. We acknowledge the support of GAČR P203/11/0442.

-
- [1] L. Skrbek and K. R. Sreenivasan, *Phys. Fluids* **24**, 011301 (2012).
 - [2] C. F. Barenghi, L. Skrbek, and K. R. Sreenivasan, *Proc. Natl. Acad. Sci. USA* **111**, 4647 (2014).
 - [3] M. Raffel, C. E. Willert, S. T. Werely, and J. Kompenhans, *Particle Image Velocimetry - A Practical Guide* (Springer, Berlin, 2007).
 - [4] T. Zhang and S. W. Van Sciver, *Nat. Phys.* **1**, 36 (2005).
 - [5] G. P. Bewley, D. P. Lathrop, and K. R. Sreenivasan, *Nature (London)* **441**, 588 (2006).
 - [6] Y. A. Sergeev and C. F. Barenghi, *J. Low Temp. Phys.* **157**, 429 (2009).
 - [7] W. Guo, M. La Mantia, D. P. Lathrop, and S. W. Van Sciver, *Proc. Natl. Acad. Sci. USA* **111**, 4653 (2014).
 - [8] M. S. Paoletti, M. E. Fisher, K. R. Sreenivasan, and D. P. Lathrop, *Phys. Rev. Lett.* **101**, 154501 (2008).
 - [9] M. La Mantia, T. V. Chagovets, M. Rotter, and L. Skrbek, *Rev. Sci. Instrum.* **83**, 055109 (2012).
 - [10] M. La Mantia, D. Duda, M. Rotter, and L. Skrbek, *J. Fluid Mech.* **717**, R9 (2013).
 - [11] G. P. Bewley, M. S. Paoletti, K. R. Sreenivasan, and D. P. Lathrop, *Proc. Natl. Acad. Sci. USA* **105**, 13707 (2008).
 - [12] E. Fonda, D. P. Meichle, N. T. Ouellette, S. Hormoz, and D. P. Lathrop, *Proc. Natl. Acad. Sci. USA* **111**, 4707 (2014).

- [13] M. La Mantia and L. Skrbek, *Europhys. Lett.* **105**, 46002 (2014).
- [14] V. S. L'vov, L. Skrbek, and K. R. Sreenivasan, *Phys. Fluids* **26**, 041703 (2014).
- [15] F. Toschi and E. Bodenschatz, *Annu. Rev. Fluid Mech.* **41**, 375 (2009).
- [16] N. Mordant, A. M. Crawford, and E. Bodenschatz, *Phys. Rev. Lett.* **93**, 214501 (2004).
- [17] N. M. Qureshi, M. Bourgoïn, C. Baudet, A. Cartellier, and Y. Gagne, *Phys. Rev. Lett.* **99**, 184502 (2007).
- [18] N. M. Qureshi, U. Arrieta, C. Baudet, A. Cartellier, Y. Gagne, and M. Bourgoïn, *Eur. Phys. J. B* **66**, 531 (2008).
- [19] L. Biferale, G. Boffetta, A. Celani, B. J. Devenish, A. Lanotte, and F. Toschi, *Phys. Rev. Lett.* **93**, 064502 (2004).
- [20] I. F. Sbalzarini and P. Koumoutsakos, *J. Struct. Biol.* **151**, 182 (2005).
- [21] G. A. Voth, K. Satyanarayan, and E. Bodenschatz, *Phys. Fluids* **10**, 2268 (1998).
- [22] G. A. Voth, A. La Porta, A. M. Crawford, J. Alexander, and E. Bodenschatz, *J. Fluid Mech.* **469**, 121 (2002).
- [23] N. Mordant, A. M. Crawford, and E. Bodenschatz, *Physica D* **193**, 245 (2004).
- [24] M. P. Rast and J.-F. Pinton, *Phys. Rev. E* **79**, 046314 (2009).
- [25] M. S. Paoletti and D. P. Lathrop, *Annu. Rev. Condens. Matter Phys.* **2**, 213 (2011).
- [26] A. W. Baggaley and C. F. Barenghi, *Phys. Rev. E* **89**, 033006 (2014).
- [27] R. J. Donnelly, *Phys. Rev. Lett.* **14**, 39 (1965).
- [28] A. W. Baggaley, C. F. Barenghi, A. Shukurov, and Y. A. Sergeev, *Europhys. Lett.* **98**, 26002 (2012).
- [29] N. Mordant, P. Metz, O. Michel, and J.-F. Pinton, *Phys. Rev. Lett.* **87**, 214501 (2001).
- [30] L. Chevillard, B. Castaing, A. Arnoedo, E. Lévêque, J.-F. Pinton, and S. G. Roux, *C. R. Phys.* **13**, 899 (2012).
- [31] M. La Mantia and P. Dabnichki, *Eng. Anal. Bound. Elem.* **36**, 579 (2012).
- [32] D. R. Poole, C. F. Barenghi, Y. A. Sergeev, and W. F. Vinen, *Phys. Rev. B* **71**, 064514 (2005).
- [33] G. Careri, U. Fasoli, and F. S. Gaeta, *Nuovo Cimento* **15**, 774 (1960).
- [34] C. F. Brennen, *A Review of Added Mass and Fluid Inertia Forces* (Naval Civil Engineering Laboratory, Port Hueneme, 1982).